a

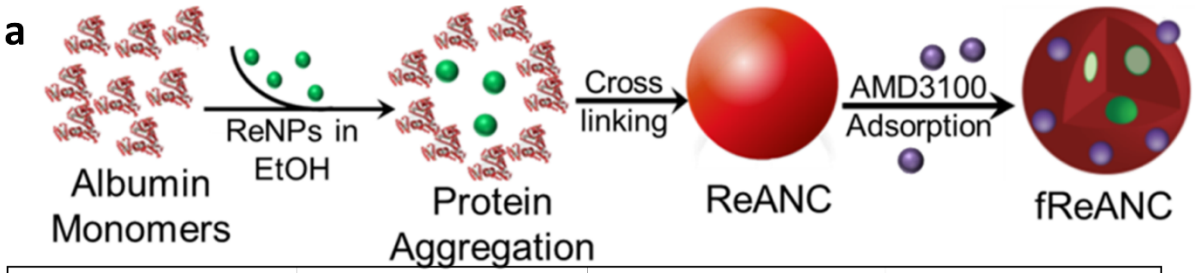

b Formulation	Size(nm)	PDI	Yield %age
ReANC	89.6 ± 3.9	0.19 ± 0.05	58.8 ± 4.1
fReANC	99 ± 8.5	0.23 ± 0.05	55.3 ± 6.1

Supplementary Figure 1: Encapsulation of rare earth cores in albumin using a solvent induced controlled coacervation process forming rare earth albumin nanocomposites (ReANCs) (a). Functionalization of the encapsulated particles to achieve active targeting to adrenal metastases, was accomplished by adsorption of AMD-3100 on to the surface of ReANCs (a). Unfunctionalized (ReANCs) and functionalized (fREANCs) nanoparticles were characterized using a zetasizer (b). The hydrodynamic diameter of the particles measured using DLS was 89.6 nm and 99 nm for ReANCs and fReANCs respectively (b). The yield of nanoparticle encapsulation measured using BCA assay was ~ 58.7% .

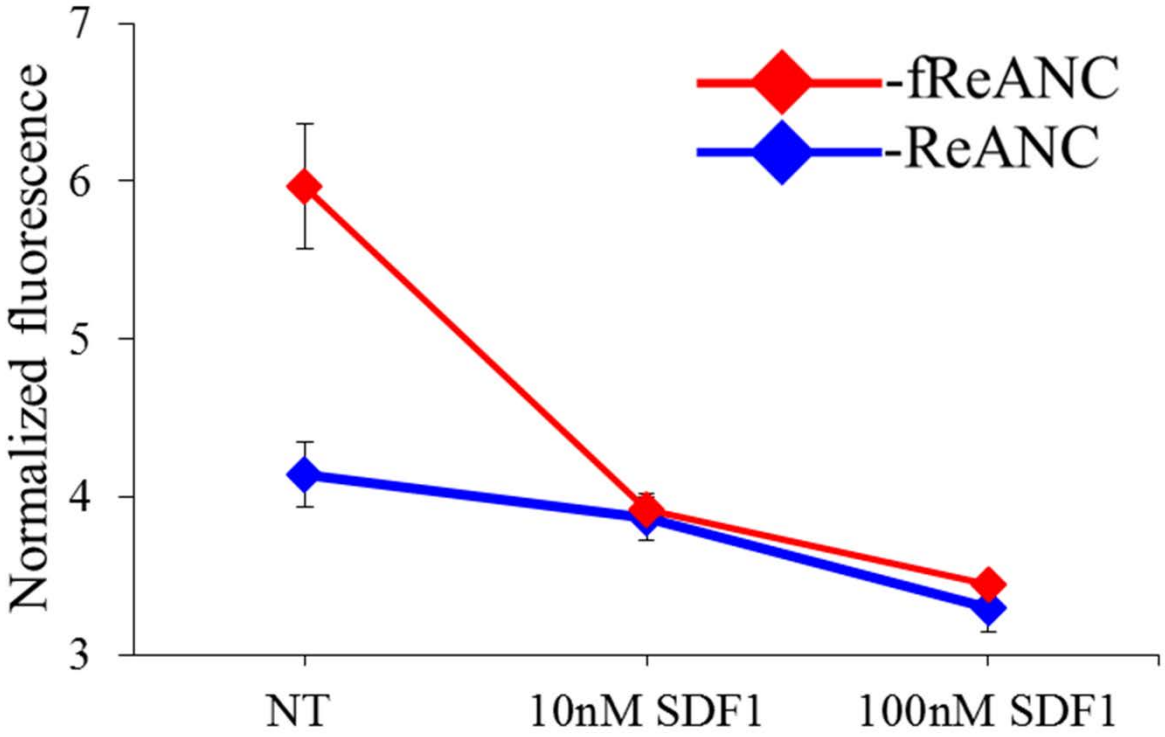

Supplementary Figure 2: Validation of the active targeting mechanism of fReANCs vis-à-vis ReANCs. Competitive inhibition using SDF1 to block CXCR4 receptors shows decreased uptake of functionalized nanoparticles compared to unfunctionalized particles in triple negative breast cancer cells. Data is represented in n=1 in triplicates as mean ± S.E.M.

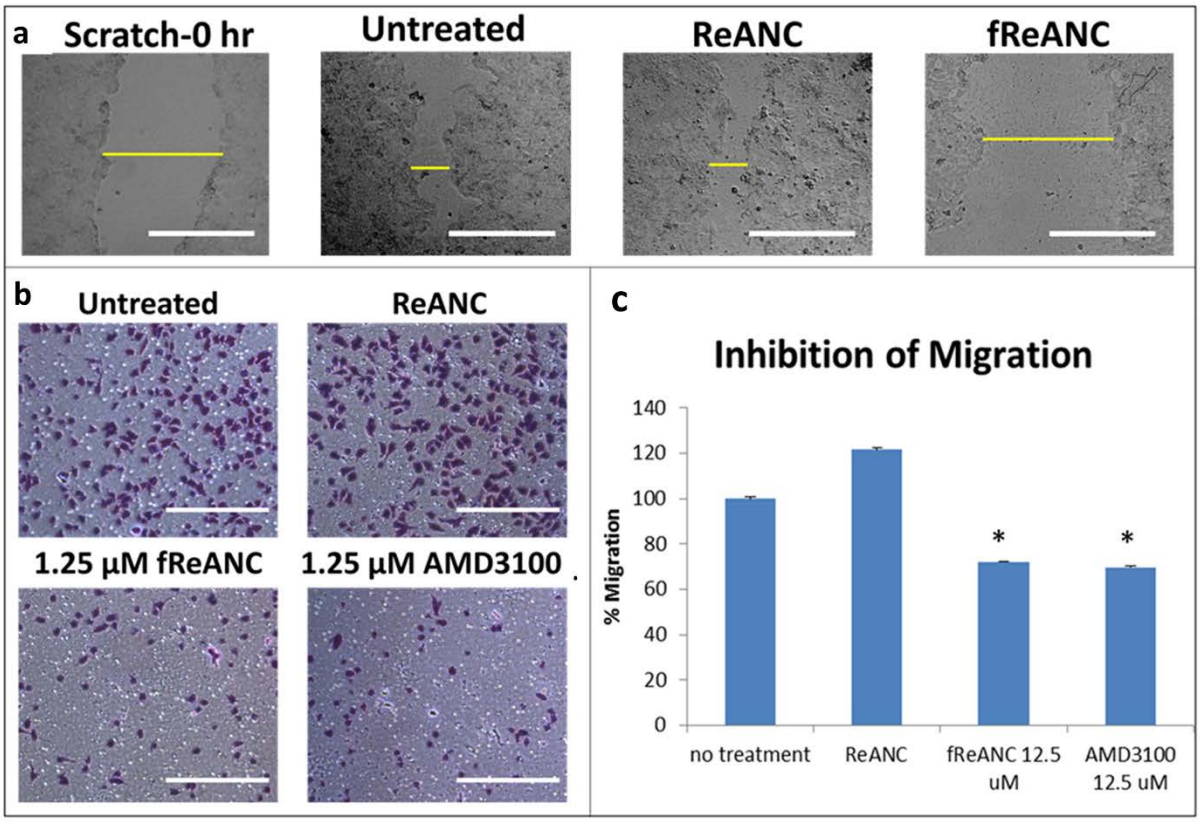

Supplementary Figure 3: Functional validation of molecular targeting features of fReANCs. In vitro, fReANC treatment was able to inhibit wound closure (A) and migration (B) of CXCR4 expressing cells, showing that CXCR4 inhibition is able to inhibit cellular metastasis. This effect was significant compared to treatment with ReANCs (C). *p<.05, n=3, one-way ANOVA, Tukey post-hoc. (A-B) scale bars 0.5 mm

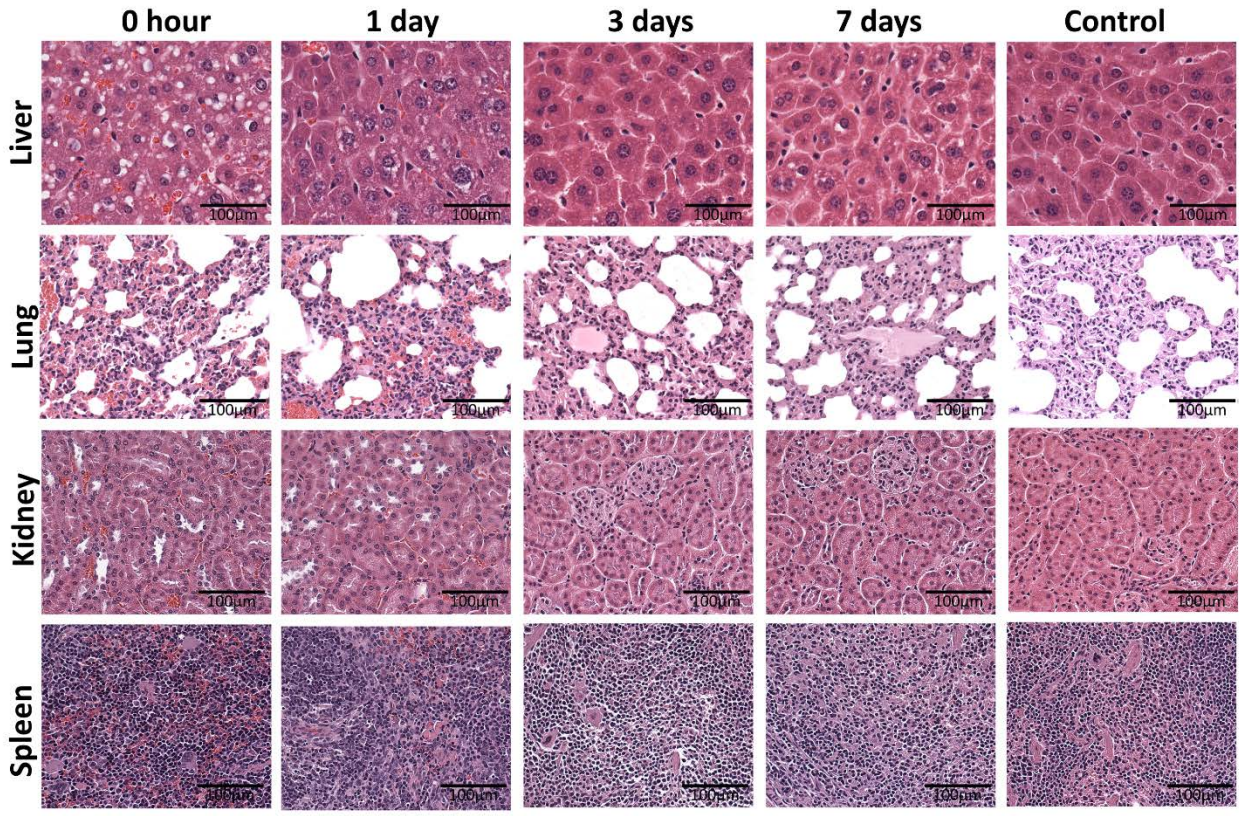

Supplementary Figure 4: Histopathological analysis of organs of clearance over time. *Ex vivo* histopathological analysis of organs excised at various time points shows no change in tissue architecture, indicating the safety of nanoprobes over time. Animals (n=5 per time-point) were sacrificed at 0 h, 24 h, 3 days and 7 days post-injection and organs of major clearance (Liver, Lung, Kidney and Spleen) were collected for H&E analysis. Representative Images from excised organs are presented to show no change in tissue architecture over time.

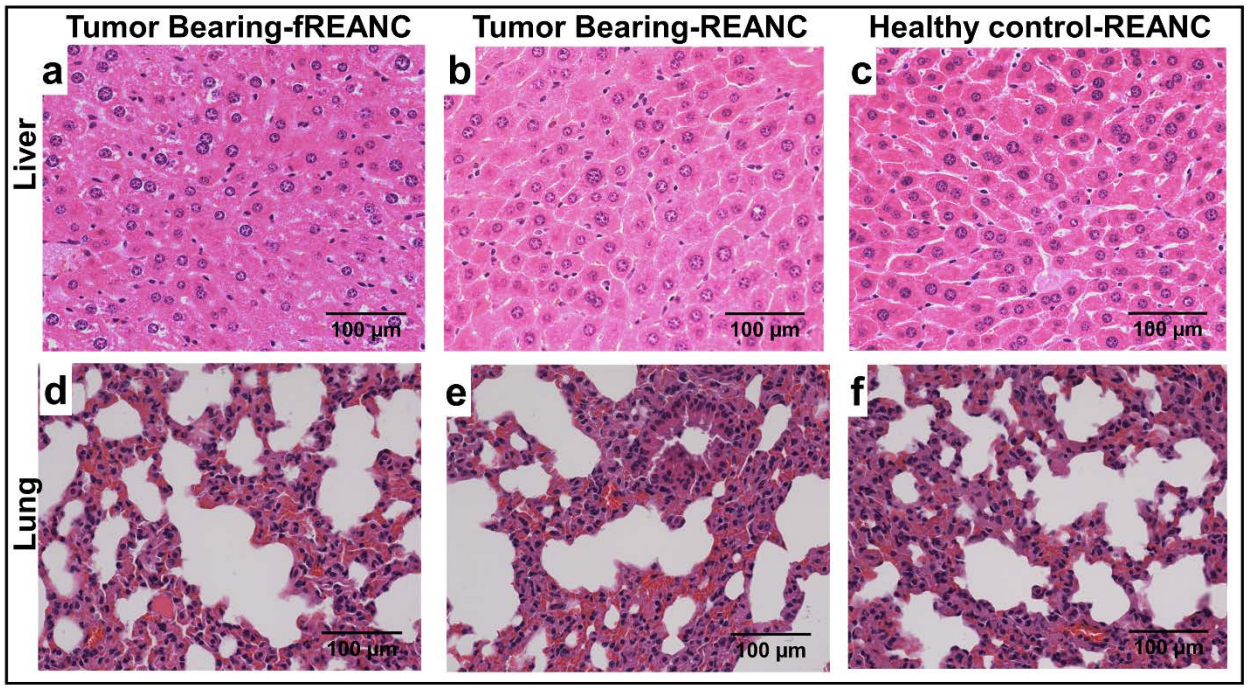

Supplementary Figure 5: Histopathological evaluation of organs of clearance for toxicity with repeated nanoparticle administration. Animals received intracardiac injections of MCF7-5624A. Tumor bearing and healthy animals received ReANC and fReANC weekly injections. Livers of tumor bearing animals receiving weekly injections of fReANC (a) and ReANC (b) were sectioned at the end point and were stained with H&E. There were no significant changes between animals treated with fReANC and ReANC and there was no loss of tissue integrity. Liver sections from healthy animals treated with ReANCs (c) also did not show any signs of damage. Additionally, lungs of tumor bearing animals injected with ReANCs (d) and fREANC (e) showed no signs of changes in lung architecture, similar to those in healthy animals injected with ReANC (f).

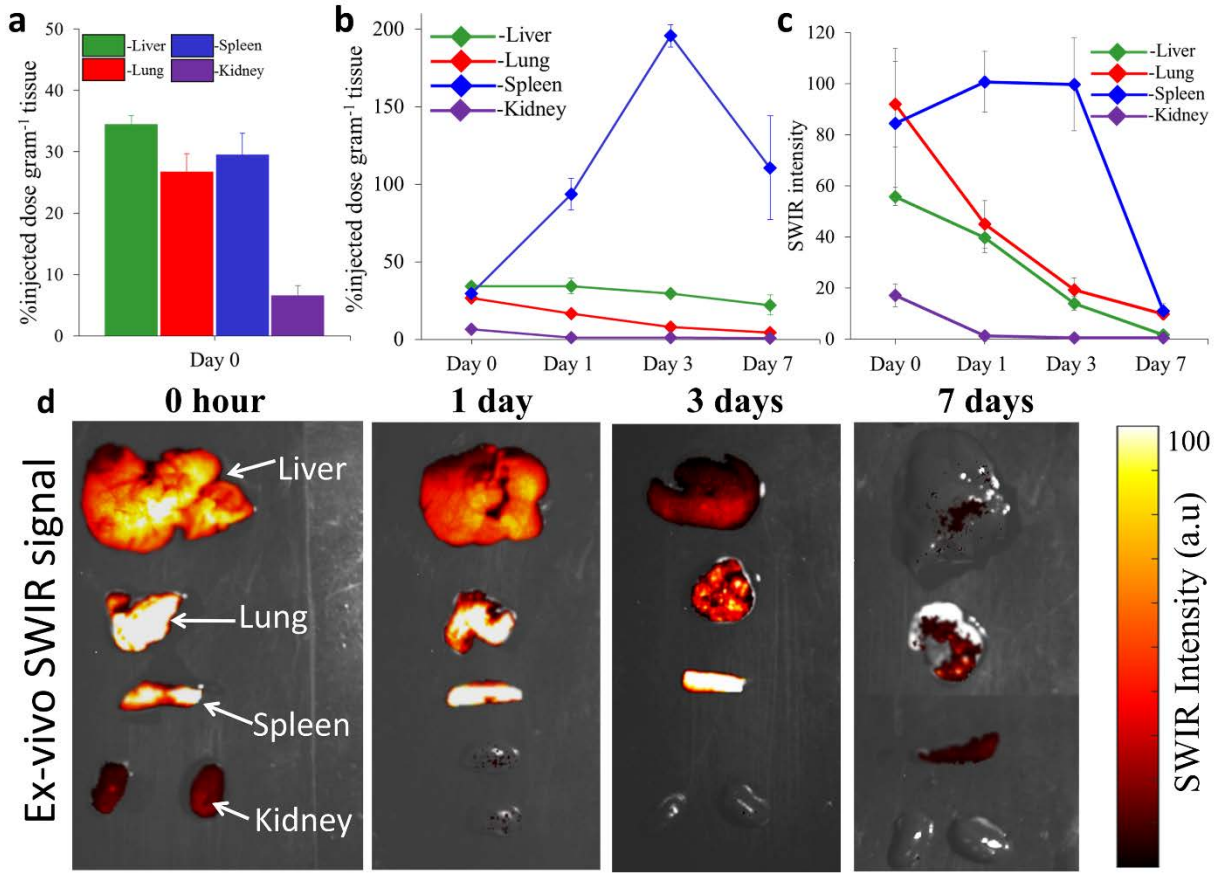

Supplementary figure 6: Quantitative clearance studies highlight effective clearance of nanoprobes. (a) ICP/MS analysis of organs of major clearance at 0, 24h, 72h and 7 days show effective clearance of particles from all organs and a decreasing trend of probe RE content in the spleen. This correlates with the SWIR signal acquired over time from the excised organs (b). The biodistribution of the nanoprobes, calculated using ICP-MS, immediately after injection indicates major accumulation in liver, lungs and spleen as shown in (c). (d) Ex vivo SWIR signal validates the clearance of the probes from the major organs of clearance over time. Data are representative means of n=5 animals per time-point represented as mean ± S.E.M.

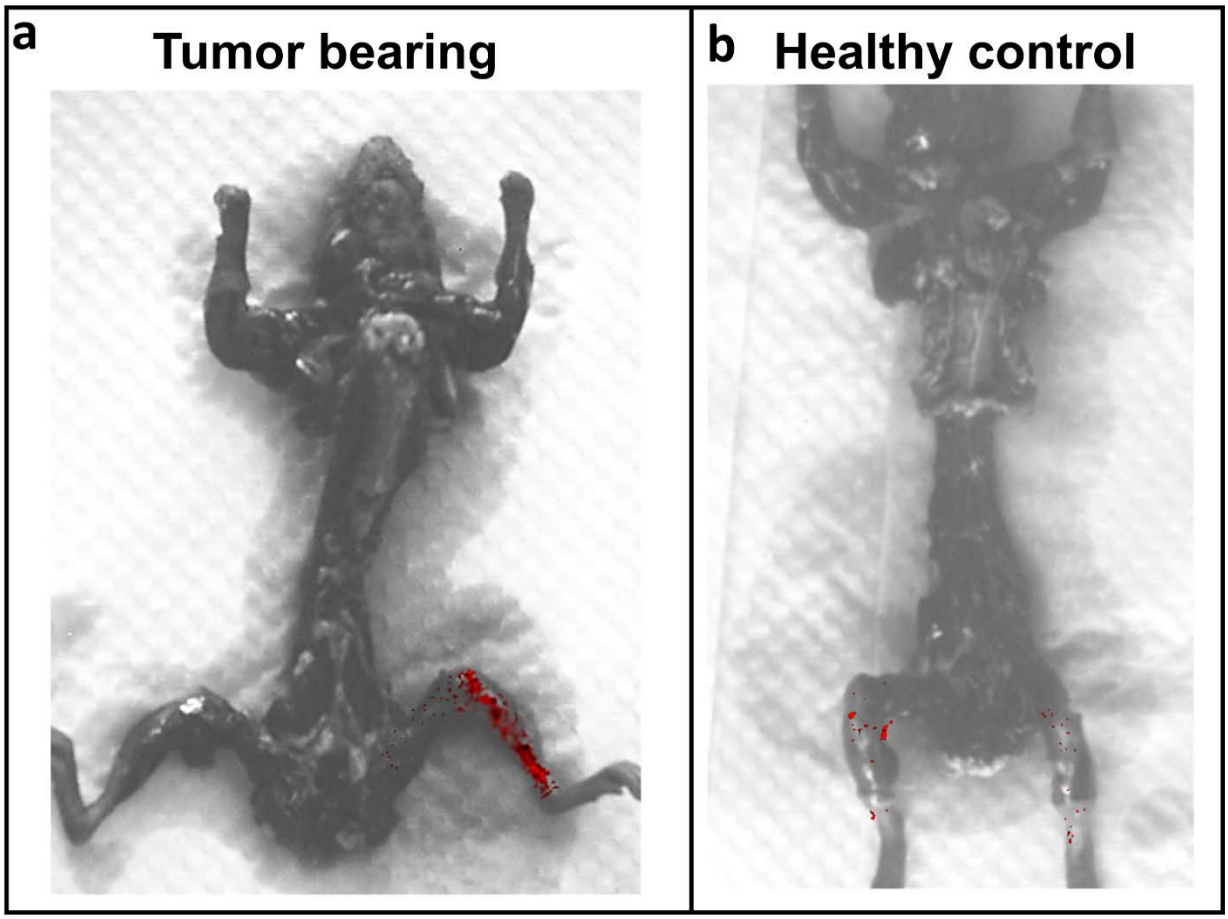

Supplementary Figure 7: *Ex vivo* validation of ReANCs in bones. Athymic nude mice were injected with MDA-MB-231 derived cells in the left tibiae followed by weekly intravenous injections of ReANCs. *Ex vivo* SWIR imaging of skeletons injected with ReANCS showed accumulation of ReANCs in bones of tumor bearing animals (a) compared to healthy controls (b).

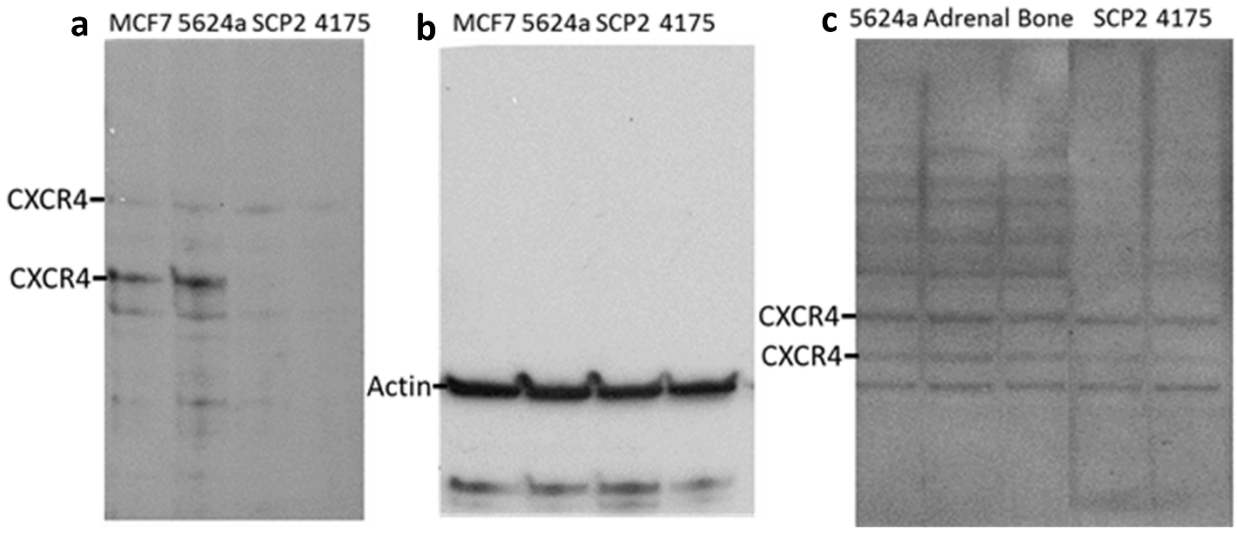

Supplementary Figure 8: Expression levels of CXCR4 in breast cancer cell lines. Western analysis shows a higher expression of CXCR4 receptor in MCF7 and MCF7-5624A breast cancer cells as compared to SCP2 or 4175 cell lines (a). Cells extracted from adrenal metastases and bone metastases also showed expression of CXCR4. The adrenal and bone tumor cells retain the same level of expression of CXCR4 as the parental MCF7-5624A cell line (b).

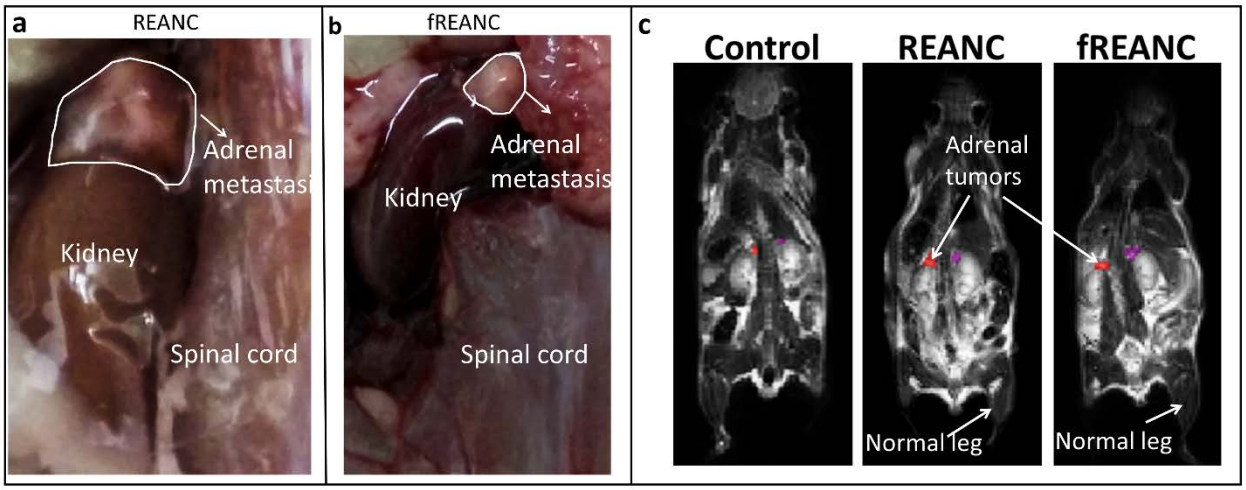

Supplementary Figure 9: MRI and *In situ* white light images indicate the presence of adrenal tumors. Animals inoculated with MCF7-5624A breast cancer cells via intracardiac injection were administered weekly doses of either REANC or fREANCs. Dissection of animals at the end point revealed the presence of enlarged adrenal glands in animals administered with (a) ReANC and (b) fReANCs compared to healthy controls (data not shown). (c) Representative MRI images of animals showing adrenal metastases and a lack of changes in bone architecture indicating the sensitivity of SWIR imaging in detecting bone metastasis.

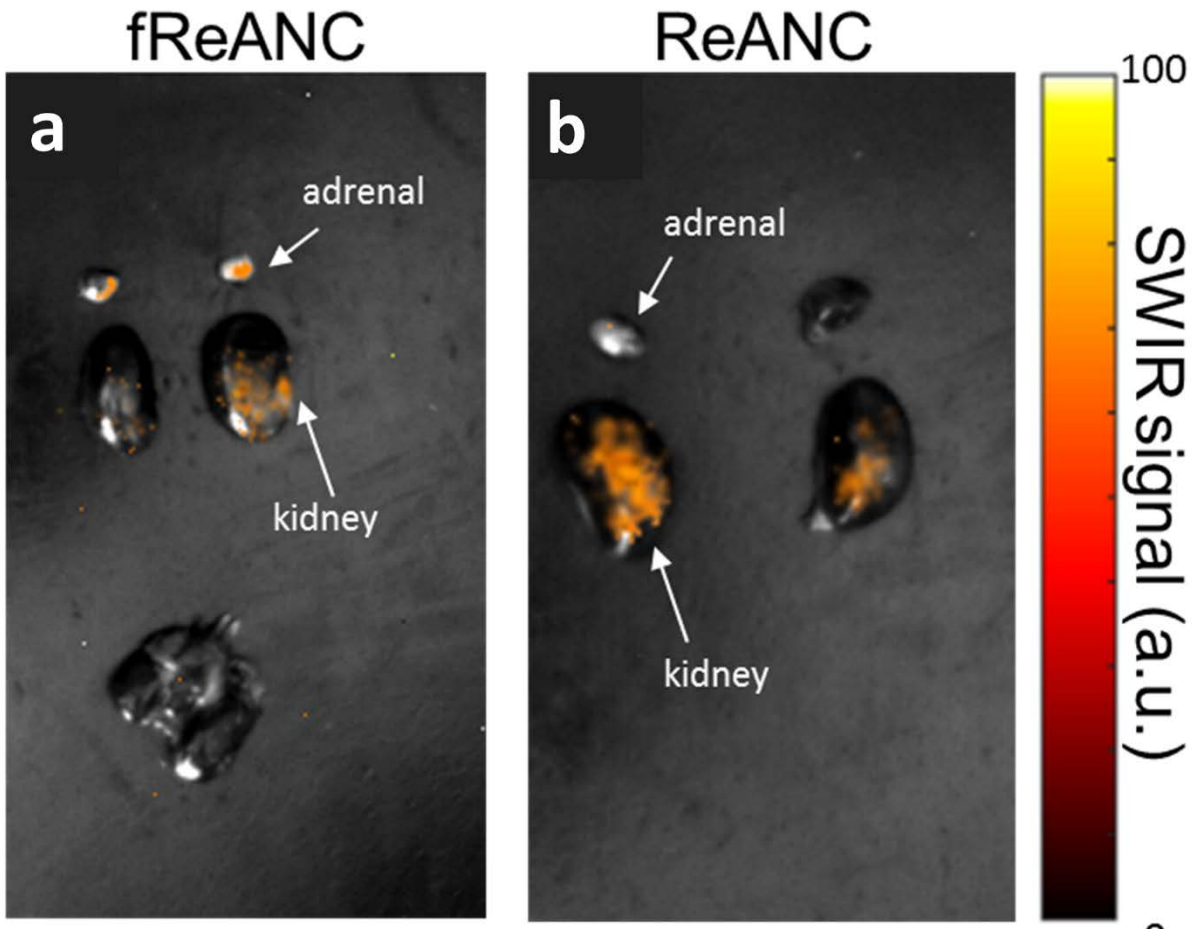

c	ReANC	fReANC*	Control
Fold Increase in SWIR Signal	5.58 ±2.84	7.31±2.89	1±.12

Supplementary Figure 10: Ex-vivo images showing presence of SWIR signal in adrenal glands of tumor bearing mice.- Animals inoculated with MCF7-5624A breast cancer cells via intracardiac injection were administered weekly doses of either REANC or fREANCs. Post sacrifice at week 5 , SWIR imaging was performed on excised organs to determine the location of probe accumulation. Enhanced levels of SWIR fluorescence was observed from the adrenal glands of mice administered with functionalized fReANCs (a) whereas less SWIR signal could be resolved from the tumors of animals administered ReANCs (b). Administration of fReANCs led to a 7.3 fold increase in SWIR signal from adrenal lesions when compared to healthy controls (c) *p<0.15, n=6, t-test, whereas the increase in SWIR signal with REANC administration was not significant as compared to healthy controls.

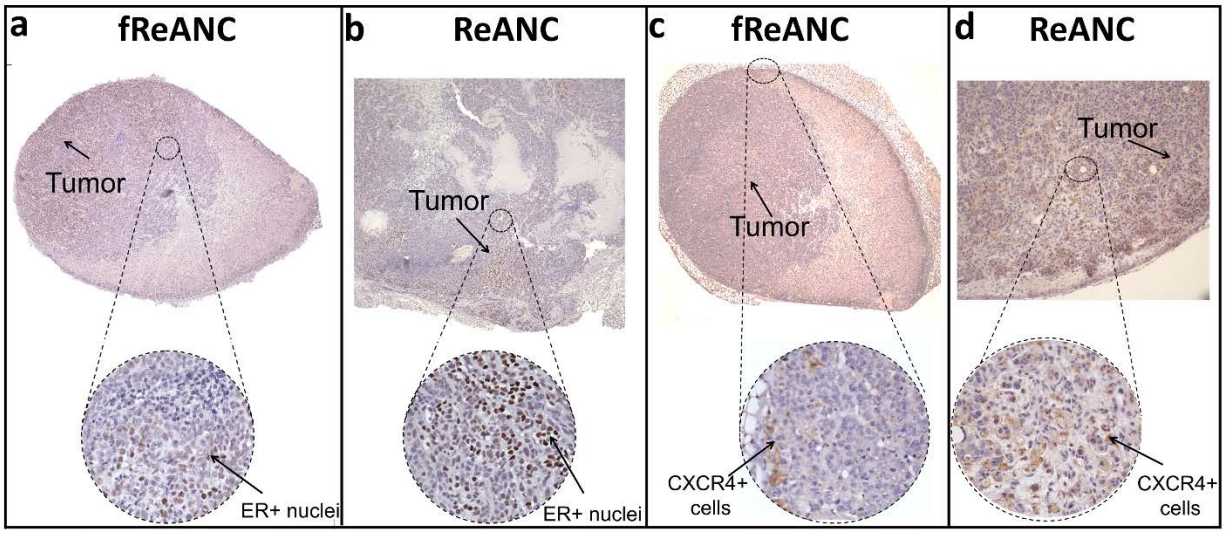

Supplementary Figure 11: Histopathological validation of ER-positive tumor cells in adrenals. *Ex vivo* immunohistochemical analysis of the adrenals verified the presence of tumor by positive estrogen receptor staining of tumor cells (a). Both tumor bearing groups injected with ReANCs and fReANCs (a & b) stained positive for the estrogen receptor. Adrenal metastases from animals injected with both ReANCs and fReANCs (c and d) also stained positive for CXCR4, as indicated by arrows.

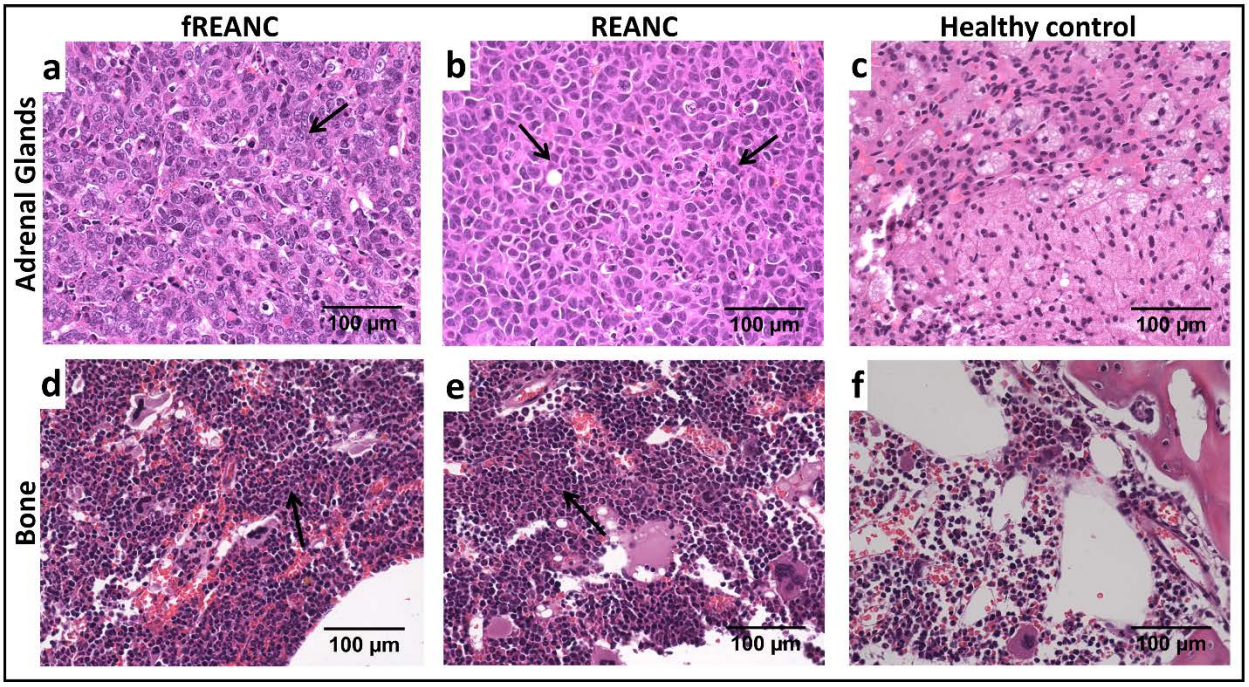

Supplementary Figure 12 - H and E staining of adrenal metastases. Adrenals from tumor-bearing animals (a and b) show the presence of irregular nuclei (shown by arrows) quite distinct when compared to healthy control (c). These structural changes are consistent with possible tumor infiltration. The H and E stains of bone structures of tumor bearing (d and e) in contrast with healthy control (f) shows possible hypo-cellularization indicative of presence of osteolytic lesions.

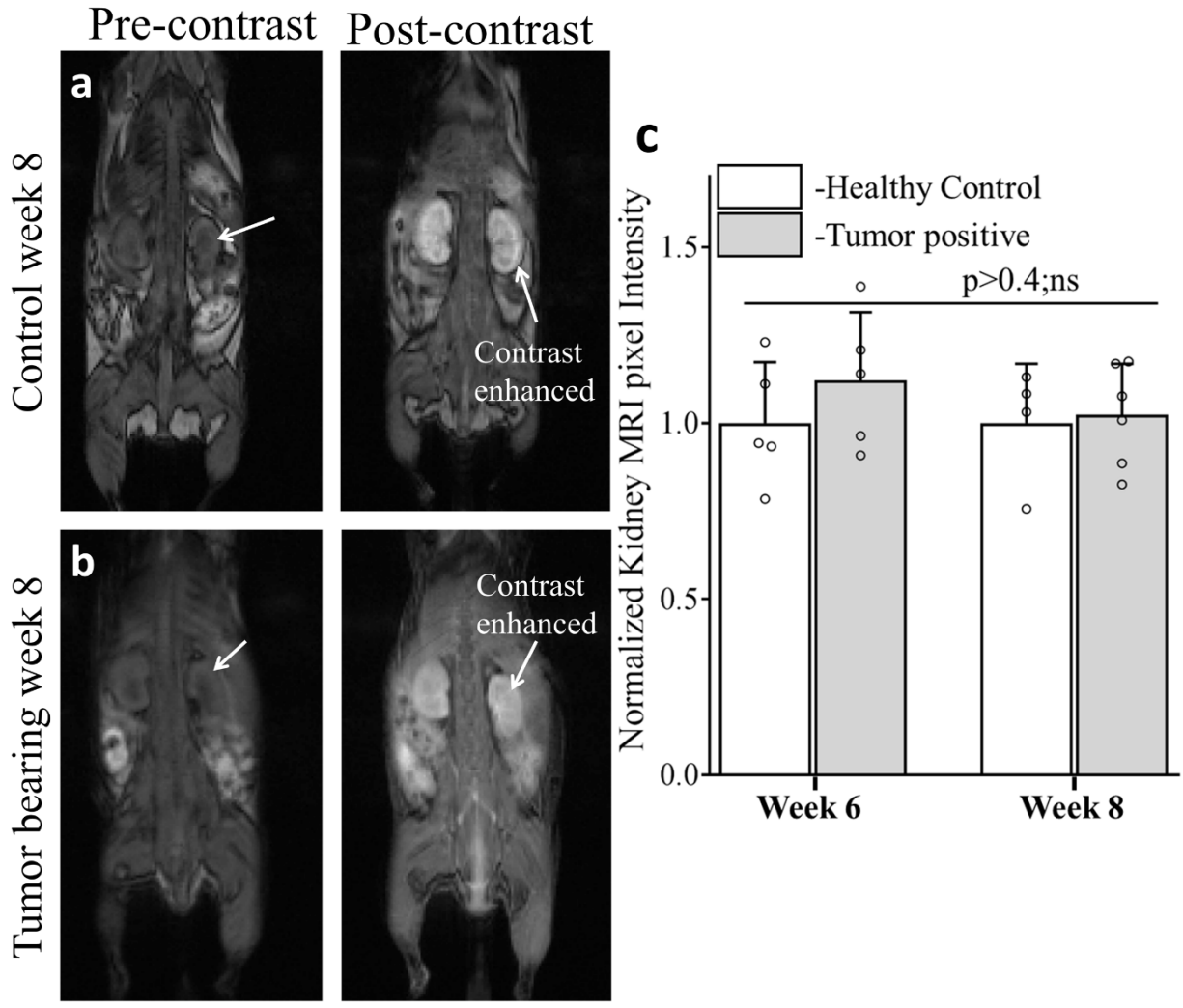

Supplementary Figure 13: Validation of contrast uptake by tumor bearing and healthy animals. Absence of change in contrast uptake by kidneys in tumor bearing (a) versus control animals (b) is shown in representative images at week 8 and (c) quantitative comparison shows no significant difference in average pixel intensity in kidneys between tumor bearing and control animals.

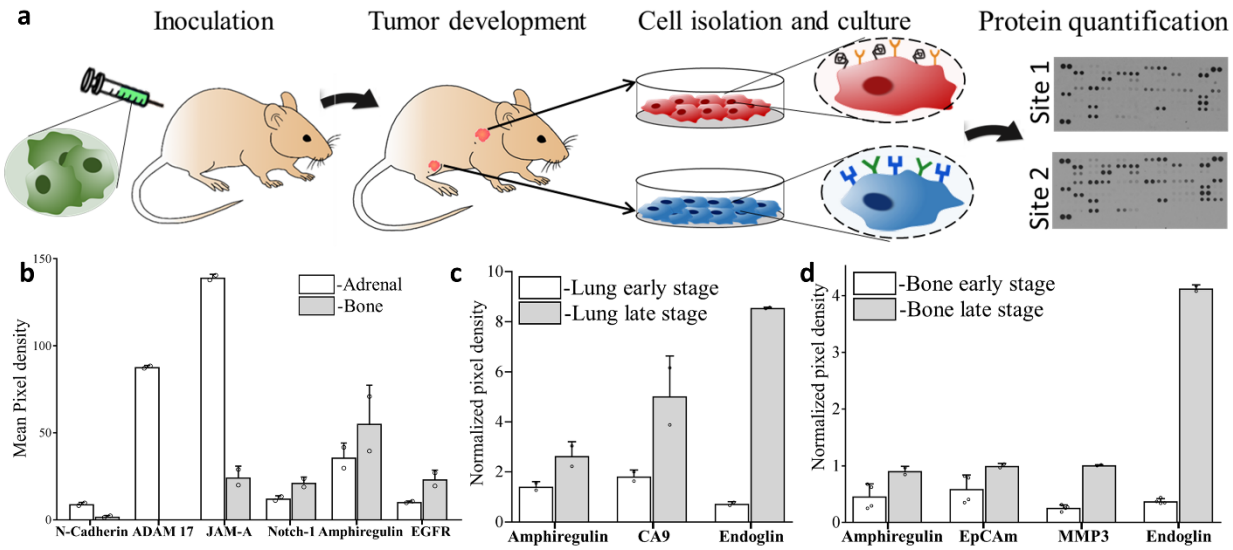

Supplementary Figure 14: Variations in molecular signatures based on metastatic niche: (a) Cells were isolated and cultured from tumor tissues excised from multiple metastatic sites in the animal. Differential expression of proteins in various niches was determined using human soluble receptor array and human oncology array as described under materials and methods. Differences in protein expression were quantified based on antibody array pixel density. (b) Fold changes in protein expression calculated using difference in pixel density indicate the variations of protein expression between adrenal and bone tropic cell lines. We also determined protein expression changes at early (2weeks post-inoculation) and late (6weeks post-inoculation) stages of tumor progression. Fold changes in protein expression in lung tropic cell line(c) and bone tropic lines (d) with progression of tumor indicate increase in proteins involved in tumor invasiveness and metastatic ability.

Supplementary Video 1: Real time SWIR imaging of athymic nude mice injected with 200ul of ReANCs intravenously imaged in supine position. Whole body imaging of the animal was performed using an InGaAs camera (Sensors Unlimited, Princeton, NJ) equipped with two 1020 long pass filters and one 1538/82 filter to resolve the emission specifically from ReANCs. The video captured at 20 frames/second highlights the SWIR emission from ReANC probes in the tail vein (site of injection), the long bones in the hind limbs, the liver (the primary organ of clearance) and the spine.